

# Identification of a novel deFADding activity in human, yeast and bacterial 5' to 3' exoribonucleases

Sunny Sharma<sup>1,†</sup>, Jun Yang<sup>1,†</sup>, Selom K. Doamekpor<sup>2</sup>, Ewa Grudizen-Nogalska<sup>1</sup>, Liang Tong<sup>2</sup> and Megerditch Kiledjian<sup>1,\*</sup>

<sup>1</sup>Department of Cell Biology and Neurosciences, Rutgers, University, Piscataway, NJ 08854, USA and <sup>2</sup>Department Biological Sciences, Columbia University, New York, NY 10027, USA

Received March 31, 2022; Revised June 18, 2022; Editorial Decision June 27, 2022; Accepted July 21, 2022

## ABSTRACT

Identification of metabolite caps including FAD on the 5' end of RNA has uncovered a previously unforeseen intersection between cellular metabolism and gene expression. To understand the function of FAD caps in cellular physiology, we characterised the proteins interacting with FAD caps in budding yeast. Here we demonstrate that highly conserved 5'-3' exoribonucleases, Xrn1 and Rat1, physically interact with the RNA 5' FAD cap and both possess FAD cap decapping (deFADding) activity and subsequently degrade the resulting RNA. Xrn1 deFADding activity was also evident in human cells indicating its evolutionary conservation. Furthermore, we report that the recently identified bacterial 5'-3' exoribonuclease RNase AM also possesses deFADding activity that can degrade FAD-capped RNAs *in vitro* and in *Escherichia coli* cells. To gain a molecular understanding of the deFADding reaction, an RNase AM crystal structure with three manganese ions coordinated by a sulfate molecule and the active site amino acids was generated that provided details underlying hydrolysis of the FAD cap. Our findings reveal a general propensity for 5'-3' exoribonucleases to hydrolyse and degrade RNAs with 5' end noncanonical caps in addition to their well characterized 5' monophosphate RNA substrates indicating an intrinsic property of 5'-3' exoribonucleases.

## INTRODUCTION

Regulation of gene expression in consonance with metabolic state is critical for cell survival. This coordination between metabolism and gene expression is driven by several key metabolites, particularly adenine-containing nucleotide metabolites such as nicotinamide adenine dinucleotide (NAD), flavin adenine dinucleotide (FAD),

coenzyme A (CoA) and *S*-adenosyl methionine (SAM) (1). These metabolites generally function as cofactors or co-substrates for many enzymes that modify chromatin and play key tasks in both activation and repression of gene expression (2).

Recent identification of NAD as an RNA 5' end cap in bacteria (3), yeast (4), plants (5,6) and mammals (7) has uncovered a unique metabolic network where a metabolite can directly influence gene expression. Both structural and biochemical analyses in prokaryotes have revealed that RNA polymerases can use NAD in place of ATP at the 5' end during transcription initiation (8). In contrast, an NAD cap on post-transcriptionally processed intronic small nucleolar RNAs (snoRNAs) in mammalian cells has highlighted an alternative mechanism of a post-transcriptional NAD capping (7). Recent studies in model organisms representing both prokaryotes and eukaryotes led to the identification of different NAD cap decapping (deNADding) enzymes that has aided in understanding the biological function of NAD caps (3,5,7,9,10). In prokaryotes, specifically in *Escherichia coli*, the NAD cap protects RNA from 5' end degradation (3), whereas in mammals, the NAD cap serves as a mark to degrade the RNA at least in part by the DXO deNADding followed by 5'-3' exoribonuclease activities (7). More recently, characterization of NAD cap binding proteins in yeast led to the identification of the highly conserved Xrn1 and Rat1 5'-3' exoribonucleases as novel deNADding enzymes and revealed a central role of NAD-capped RNAs in mitochondrial function (11).

In addition to NAD caps, chemical analysis of the RNA 5'-cap epitranscriptome using LC-MS/MS based CapQuant (12) from different organisms revealed that mRNAs also contain other metabolite caps like FAD, dephosphoCoenzyme A (dpCoA), Uridine diphosphate glucose (UDP-Glc), and Uridine diphosphate *N*-acetylglucosamine (UDP-GlcNAc). Nevertheless, the function of these metabolite caps in RNA metabolism remained elusive. It is important to note that identification of the enzymatic machinery involved in addition and removal of these metabolite caps is imperative to under-

\*To whom correspondence should be addressed. Tel: +1 848 445 0796; Email: [kiledjian@biology.rutgers.edu](mailto:kiledjian@biology.rutgers.edu)

†The authors wish it to be known that, in their opinion, the first two authors should be regarded as Joint First Authors.

standing their biological function. Our initial screening of putative metabolite cap decapping enzymes for FAD cap (deFADding) led to the identification of Rai1 along with its mammalian homolog DXO (13), and two NUDIX proteins Nudt2 and Nudt16 as deFADding enzymes (10).

In the present study, we performed FAD cap RNA affinity purification (FcRAP) and identified novel FAD cap associated proteins in budding yeast. Interestingly, in addition to their role in hydrolyzing NAD-capped RNA (11), Xrn1 and Rat1 are potent deFADding enzymes. Furthermore, a recently reported 5'-3' exoribonuclease, RNase AM (ycaV) (14,15) in *E. coli* is also capable of deFADding and hydrolyzing FAD capped RNA and its crystal structure reveals the organization of its active site. Our studies suggest a potential commonality of 5'-3' exoribonucleases towards FAD-capped RNA hydrolysis and decay in both prokaryotes and eukaryotes.

## MATERIALS AND METHODS

### FAD cap RNA affinity purification (FcRAP)

The *in vitro* transcribed FAD and m<sup>7</sup>G capped RNAs (~400 pmol) were immobilized onto Dynabeads™ MyOne™ Strep-tavidin T1 (Invitrogen™). Yeast cells (Supplementary Table S3) were grown and processed as described recently (11). Briefly, 5 mg of protein lysate was added to the pre-equilibrated (in 1 × lysis buffer) FAD- or m<sup>7</sup>G-capped RNA linked Dynabeads in 2 ml microcentrifuge tubes. These tubes were next incubated at 4°C on an end-to-end rocker for 90 min. After extensive washing (at least 5 times with 1 × lysis buffer) the associated proteins were eluted with 2 × Laemmli buffer (Bio-Rad Laboratories). The samples were denatured at 85°C for 5 min and were next run on Novex™ WedgeWell™ 4–20 %, Tris–glycine protein gel (Thermo Fisher Scientific). The protein gel was stained with SYPRO Ruby (Bio-Rad Laboratories) or with silver staining as described before (16), and specific bands were sliced and processed for mass spectrometry-based identification. In addition to the individual sliced bands from a minimum of three biological replicates, we also examined the total eluate using mass spectrometry. Complete list of identified proteins is provided in the Supplementary Table S1.

Mass spectrometry was carried out at the Biological Mass Spectrometry Facility of Robert Wood Johnson Medical School and Rutgers, The State University of New Jersey and as described previously (11). Thermo Proteome Discoverer (v. 2.1) was used to generate the peak list of the LC–MS/MS into MASCOT Generic Format (MGF) and searched against the uniprot yeast fasta database and a database composed of common lab contaminants (CRAP) using in house version of X!Tandem (GPM Fury (17)). We used these search parameters: fragment mass error, 20 ppm; parent mass error, ±7 ppm; fixed modification, carbamidomethylation on cysteine; variable modifications: methionine monooxidation for the primary search, asparagine deamination, tryptophan oxidation and dioxidation, Methionine dioxidation, and glutamine to pyroglutamine were considered at the refinement stage. Protease specificity: trypsin C-terminal of R/K unless followed by P with 1 missed cleavage during the preliminary search and 5 missed cleavages during refinement. Minimum acceptable

peptide and protein expectation scores were set at 10<sup>-2</sup> and 10<sup>-4</sup>, respectively. The overall peptide false positive rate (18) was 0.07%. The mass spectrometry values refer to spectral counts of unique plus razor peptides (peptides that have been allocated to the protein group with the largest number of total peptides identified). We applied 15 counts as a cutoff to distinguish nonspecific interactors and contaminants. This data is presented as a separate sheet (Cutoff-15) in Supplementary Table S1 along with the raw data.

### Electrophoretic mobility shift assay

Recombinant *K. lactis* Xrn1 (2.5, 5 and 7.5 pmol) was mixed with a fixed concentration (5 pmol) of <sup>32</sup>P uniformly labeled NAD- or FAD- or pA- *in vitro* transcribed RNA in 1 × RBB buffer (10 mM Tris–HCl pH7.5, 150 mM KCl, 1.5 mM MgCl<sub>2</sub> and 0.5 mM DTT) and incubated on ice for 30 min. The samples were resolved on to a 6% acrylamide gel using 0.5 × TBE at 120 V for 2–3 h. The dried gel was exposed to phosphor screen overnight and visualized with an Amersham Typhoon RGB Biomolecular Imager (GE Healthcare Life Sciences).

### Plasmid construction and site-directed mutagenesis

All proteins used in the present study for *in vitro* assays were purified as described previously (19). For RNase AM, complete ORF was cloned into a modified pET28a vector, in-frame with an N-terminal 6xHis-tagged yeast SMT3 SUMO gene using In-Fusion® Snap Assembly (TaKaRa Bio). For the construction of different point mutants, site directed mutagenesis were performed using SPRINP (20) as described previously using the oligonucleotides listed in the Supplementary Table S2.

### Protein expression and purification

All recombinant proteins—K1 Xrn1, Hs Xrn1 and RNase AM along with the mutants were expressed and purified using Nickel-NTA affinity purification (Supplementary Table S3). 10 ml LB cultures containing 50 µg/ml kanamycin were inoculated with single colonies and grown overnight. For purification, 1 l LB culture was grown at 37°C to an OD<sub>600</sub> of 0.5. Protein expression was induced with 0.25 mM isopropyl D-thiogalactopyranoside (IPTG) and cells grown at 18°C on a shaker for ~18 h. Cells were collected by centrifugation at 5000 g for 15 min, washed with PBS. For protein purification, cell pellets were resuspended in ~60 ml of buffer (25 mM HEPES (pH 7.5), 250 mM KCl, 10% glycerol, and 100 µM MnCl<sub>2</sub>) containing 0.4 mg/ml protease inhibitor phenylmethanesulfonylfluoride fluoride (PMSF). Cells were lysed by sonication, and the insoluble cell debris was separated by centrifugation. The nickel-NTA affinity purification was performed as described previously (19).

### *In vitro* transcription of NAD-, FAD-capped RNAs

NAD, FAD and m<sup>7</sup>G cap containing RNAs were synthesized by *in vitro* transcription from a synthetic double stranded DNA template Φ2.5-NAD/FAD-40 containing the T7 Φ2.5 promoter and a single adenosine within the

**Table 1.** Summary of crystallographic information

Structure	RNase AM in complex with Mn and sulfate
<b>Data collection</b>	
Space group	<i>P</i> 2 <sub>1</sub>
Cell dimensions	
<i>a</i> , <i>b</i> , <i>c</i> (Å)	40.3, 74.4, 40.1
$\alpha$ , $\beta$ , $\gamma$ (°)	90, 119.0, 90
Resolution (Å)	35.24–1.70 (1.75–1.70)
<i>R</i> <sub>merge</sub> (%)	13.7 (74.4)
CC <sub>1/2</sub> (%)	98.7 (78.1)
<i>I</i> / $\sigma$ <i>I</i>	10.0 (3.9)
Completeness (%)	97.7 (94.3)
No. of reflections	22 722 (2180)
Redundancy	5.0 (4.9)
<b>Refinement</b>	
Resolution (Å)	35.2–1.70 (1.75–1.70)
<i>R</i> <sub>work</sub> / <i>R</i> <sub>free</sub> (%)	18.2 (35.4) / 21.3 (41.8)
Number of atoms	1768
Protein	1631
Ligand/ion	8
Water	129
<i>B</i> -factors (Å <sup>2</sup> )	23.3
Protein	22.7
Ligand	18.7
Water	31.1
r.m.s.d.	
Bond lengths (Å)	0.007
Bond angles (°)	1.00
Ramachandran plot statistics	
Favored	97.0
Allowed	3.0
Outliers	0.0

transcript contained at the transcription start site (Supplementary Table S2). For m<sup>7</sup>G-capped RNA, m<sup>7</sup>GpppA RNA Cap Structure Analog (New England Biolabs) was included in the transcription reaction. *In vitro* transcription was carried out at 37°C overnight, using HiScribe™ T7 High yield RNA Synthesis kit (New England Biolabs). To generate <sup>32</sup>P uniformly labeled RNA, the transcription reactions were performed in the presence of [ $\alpha$ -<sup>32</sup>P] GTP.

### RNA *in vitro* deFADding assay.

The [ $\alpha$ -<sup>32</sup>P] GTP uniformly labeled FAD-capped RNAs were incubated with the specified amounts of recombinant protein in NEB buffer 3 (100 mM NaCl, 50 mM Tris–HCl, 10 mM MgCl<sub>2</sub>, pH 7.9). For RNase AM, 4 mM MnCl<sub>2</sub> was used instead of MgCl<sub>2</sub>. Reactions were stopped by heating at 85°C for 2 min. *In vitro* 5' end RNA decay was carried out as described (11), cell extract corresponding to 2  $\mu$ g of cellular protein from WT or *xrn1*  $\Delta$  strains were incubated with [ $\alpha$ -<sup>32</sup>P] GTP uniformly labeled FAD and m<sup>7</sup>G-capped RNA immobilized onto Dynabeads™ MyOne™ Streptavidin T1 (Invitrogen™) in NEB buffer 3.

### FAD-cap detection and quantitation (FAD-capQ)

Bacterial and yeast total RNA were extracted using hot phenol (21), whereas RNA from human cells were isolated using Trizol (Invitrogen™). The strains used in the present study are listed in Supplementary Table S3. To remove residual free FAD, purified RNAs were dissolved in 10 mM Tris–

HCl (pH 7.5) containing 2 M urea. RNA samples were incubated 2 min at 65°C and immediately precipitated with isopropanol in the presence of 2 M ammonium acetate. FAD-capQ was carried out as previously described (13). For human cells, 30  $\mu$ g of small RNAs (<200 nts) isolated using Monarch (NEB) were used. For bacteria and yeast, 50  $\mu$ g of total RNA was used for the FAD-capQ analysis.

To demonstrate the release of intact FAD upon Xrn1 or RNase AM mediated deFADding of FAD capped RNAs, FAD-capQ assay using different amounts of *in vitro* transcribed FAD capped RNA was used. For the Xrn1 hydrolysis reactions, 100 mM of the WT or E178Q catalytic-inactive mutant Xrn1 was used. For RNase AM, 150 nM of WT or catalytically-inactive D20A mutant was used.

### Structure determination

An expression construct for full-length *E. coli* RNase AM was used to transform *E. coli* BL21 (DE3) Rosetta cells. His-tagged RNase AM was produced and purified like previously reported (14). Prior to induction with 0.25 mM IPTG, the iron-specific chelator 2,2'-bipyridyl was added to a final concentration of 0.15 mM for 30 minutes followed by the addition of MnSO<sub>4</sub> at 1 mM. After cell disruption by sonication and centrifugation, the lysate (in a buffer containing 250 mM NaCl, 20 mM Tris (pH 7.5), 20 mM imidazole, 5 mM  $\beta$ -mercaptoethanol (BME), 10% (v/v) glycerol, 0.1 mM MnSO<sub>4</sub> and 1 mM phenylmethanesulfonylfluoride (PMSF)) was incubated with 2 ml of Ni-NTA superflow resin (Qiagen) with nutation for 1 h. RNase AM was eluted with 5 ml of buffer containing 250 mM NaCl, 20 mM Tris (pH 7.5), 250 mM imidazole, 5 mM BME, 10% (v/v) glycerol and 0.1 mM MnSO<sub>4</sub> and further purified with gel filtration (Superdex 200, Cytiva Life Sciences) chromatography (in buffer containing 200 mM NaCl, 20 mM Tris (pH 7.5) and 2 mM DTT).

Attempts to crystallize RNase AM alone or supplemented with FAD did not yield diffraction quality crystals. Good-quality RNase AM crystals were obtained in the presence of dsRNA (5' GUUGUUCUCUACGAAGAACU3'; from the constitutive decay element of IL6 (22)) using the sitting-drop vapor diffusion method at 20°C with a reservoir solution containing 20% (w/v) PEG 8000 and 0.1 M HEPES pH 7.0. RNase AM crystals were cryo-protected with 20% (w/v) PEG 8000 and 25% (v/v) ethylene glycol before being flash frozen in liquid nitrogen for diffraction analysis and data collection at 100 K. X-ray diffraction data were collected at the Advanced Photon Source (APS) beamline 24-ID-C. The diffraction images were processed and scaled with standard parameters using the XDS program (23). The crystal belongs to space group *P*2<sub>1</sub>.

Molecular replacement (MR) using full-length amidohydrolase from *Chromobacterium violaceum* (PDB: 2YB1) (24) did not yield a molecular replacement solution, with the program Phaser (25). A correct MR solution could be obtained only with the PHP domain. No additional density for the insertion domain of RNase AM was observed, suggesting that it is disordered. The structure refinement was performed using PHENIX (26) and manual rebuilding of

the atomic model was carried out with the Coot program (27). The final model contains residues 9–106 and 177 to 284. Density for the 3 metal ions was assigned as manganese with a sulfate molecule in the active site and no RNA density was observed. The crystallographic information is summarized in Table 1.

## RESULTS

### Characterization of FAD cap binding proteins in budding yeast

We recently employed NAD cap RNA affinity purification (NcRAP) to characterize NAD cap binding proteins to study their biological roles (11). Similarly, to begin understanding the functional role of FAD caps, we performed 5' FAD cap RNA Affinity Purification (FcRAP). Here, an *in vitro* transcribed FAD-capped RNA containing a 3'-biotin was used as bait to capture and identify proteins associated with the FAD cap from *S. cerevisiae* lysate as illustrated in Figure 1A. Two identical RNAs that differed only at their 5' end cap (m<sup>7</sup>G or FAD cap) were used to account for common RNA-binding proteins. Affinity purified proteins associated with the different RNAs were identified by mass spectrometry and the m<sup>7</sup>G-capped RNA was used as the control. Mass spectrometry identification of proteins selectively bound to the FAD-cap (Supplementary Data 1) revealed the most prominent FAD cap associated proteins to be the 5'-3' exoribonucleases Xrn1 and Rat1 as well as the Rat1 associated deFADding protein, Rai1 (13,28) (Figure 1B). FcRAP was also carried out with protein extract derived from an Xrn1 deletion (*xrn1Δ*) strain which still retains the association of Rat1 and Rai1 but as expected is devoid of Xrn1 association (Figure 1B). Lastly, to control for the association of Rat1 to the FAD cap through its interacting protein Rai1, a similar analysis was carried out with extract devoid of Rai1 (*rai1Δ*) where Rat1 is still detected with the FAD-capped RNA (Supplementary Figure S1). These findings demonstrate all three proteins have the capacity to associate with the FAD cap. Interestingly, these three proteins were also recently shown to selectively associate with and hydrolyze the NAD cap (11).

The interaction of Xrn1 with the FAD cap was further explored using electrophoretic mobility shift assays (EMSA). Equimolar concentration of Xrn1 and uniformly labeled *in vitro* transcribed FAD- and NAD-capped RNAs along with triphosphate RNA were mixed and incubated on ice for 30 min. Xrn1 can form a stable complex with both FAD- and NAD-capped RNAs (Figure 1C) that is minimally competed by excess nonspecific competitor total yeast RNA (Figure 1D). Use of an identical control RNA containing a 5' triphosphate demonstrated nonspecific associations (Figure 1C) that were more readily competed by the competitor RNA (Figure 1D). These findings reveal Xrn1 is capable of selectively binding to both NAD and FAD caps under the assay conditions employed.

### Xrn1 and Rat1 hydrolyze FAD-capped RNAs *in vitro*

The capacity for Xrn1 and Rat1 to hydrolyze a FAD cap (Figure 2A) was next tested. This was predicated on our re-

cent demonstration that both enzymes can hydrolyze NAD-capped RNA (11). Uniformly <sup>32</sup>P-labeled FAD-capped RNA was degraded by wild-type *Kluyveromyces lactis* Xrn1 and *Schizosaccharomyces pombe* Rat1, but not their corresponding catalytically inactive mutant protein *xrn1-E178Q* and *rat1-E207Q* respectively (Figure 2B). Moreover, the decay activity of both proteins on FAD-capped RNA was processive without discernable hydrolysis intermediates. In contrast, the *S. pombe* Rai1, which lacks exonuclease activity (28), only released the FAD cap without subsequent RNA degradation (Figure 2B). Collectively, these results suggest that both Xrn1 and Rat1 utilize the same catalytic active site for the hydrolysis of FAD-capped RNA and for canonical 5'P RNA degradation.

### Xrn1 possess higher deFADding activity compared to Rat1 *in vitro*

To assess the kinetics of deFADding activity relative to the well-established 5' monophosphate (5'P) RNA degradation under the same assay conditions, we carried out time-course Xrn1 decay assays with 5'P- or FAD-capped RNAs. Intriguingly, the activity of Xrn1 on 5'P RNA was only ~1.3-fold more efficient than FAD-capped RNA at equivalent enzyme concentrations (Figure 2C). A comparison of Xrn1 hydrolysis of 5'P versus NAD-capped RNA revealed a ~20-fold slower decay of the latter relative to 5'P RNA (11) indicating a strong preference of Xrn1 for FAD-capped RNA comparable to its propensity to degrade 5'P RNA.

To further delineate the differential preference of FAD-over NAD-capped RNA by Xrn1, its degradation activity was deciphered in the presence of excess NAD/FAD or their respective RNA mimics. Consistent with the decay assays, free NAD or NAD3'P which would mimic the 5' end of an NAD-capped RNA, were inefficient in altering the decay of either 5'P- or FAD-capped RNA (Supplementary Figure S2A). Minor inhibition was observed when monitoring NAD-capped RNA. Although no inhibition was observed when using FAD or FAD3'P on 5'P RNA, inhibition of Xrn1 decay was evident on FAD-capped RNA and more prevalent on NAD-capped RNA (Supplementary Figure S2B). Moreover, the effect was more pronounced with the FAD-capped RNA mimic, FAD3'P compared to free FAD (Supplementary Figure S2B). Interestingly, inhibition was nevertheless detected when using higher concentration of FAD (Supplementary Figure S3). Collectively, the data demonstrate the deFADding activity of Xrn1 is more efficient than its deNADding activity and Xrn1 has a higher affinity to FAD-capped RNA compared to free FAD.

We next compared the activity of Rat1 on the hydrolysis of 5'P to that of FAD-capped RNA. As shown in Figure 2D, although higher concentrations of recombinant Rat1 are necessary to detect comparable decay, the efficiency of hydrolyzing 5'P RNA relative to FAD-capped RNA was ~3.7-fold, which was less efficient than that observed with Xrn1. Collectively, our results further expand the substrate RNAs regulated by Xrn1 and Rat1 beyond their well characterized 5'P RNAs (29) and their recently described NAD-capped RNA hydrolysis (11).

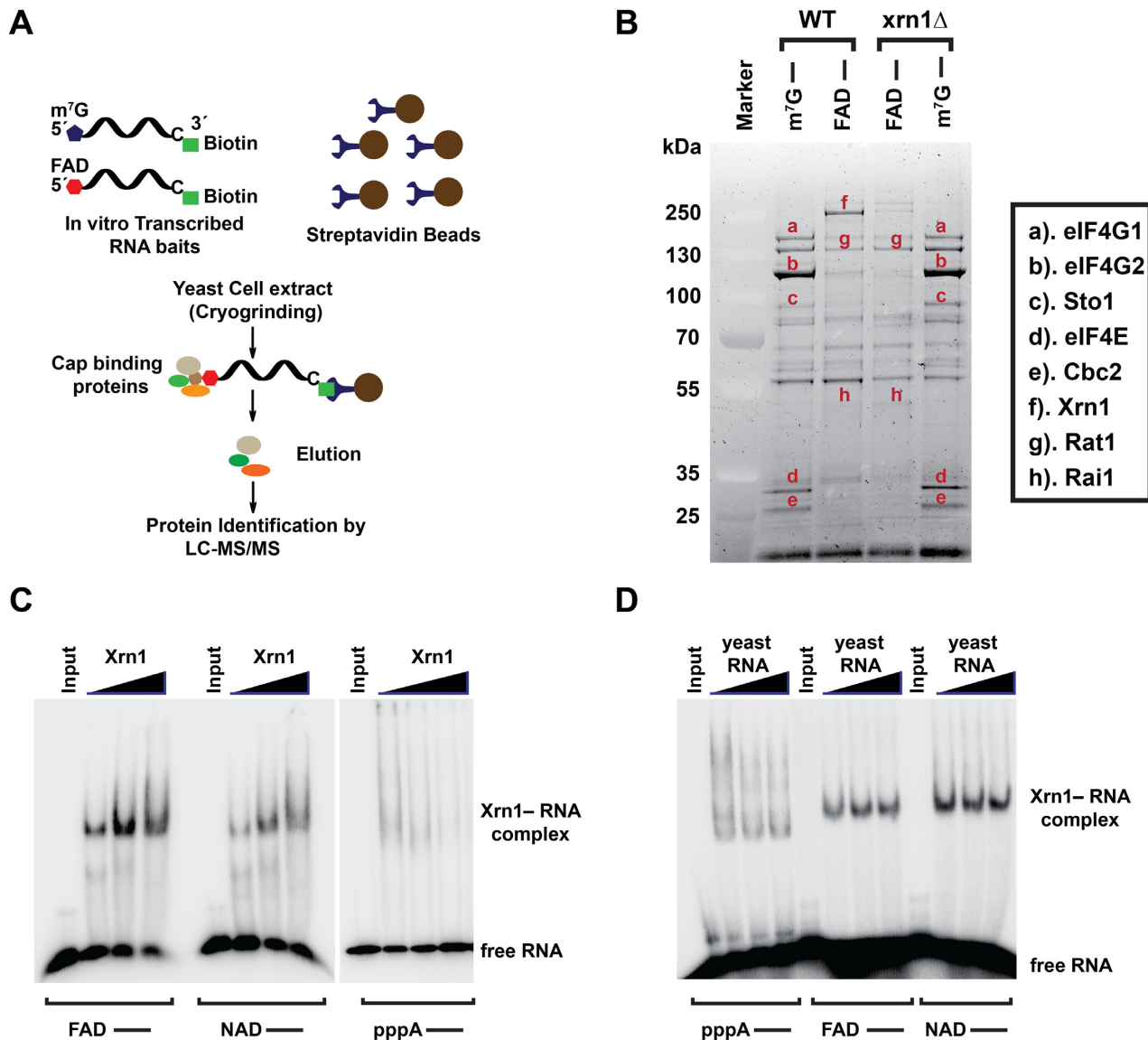


**Figure 1.** Identification of FAD cap binding proteins in budding yeast. (A) Schematic illustration of the FAD cap -RNA Affinity Purification (FcRAP). (B) Eluates from FcRAP were loaded on to a 4%-12% Bis-Tris gel and stained with SYPRO Ruby. The  $m^7G$  cap affinity purification was used as a control. All protein bands labeled on the gel were excised from the gel and identified using mass spectrometry. (C) Electrophoretic mobility shift assay (EMSA) using increasing concentration of Xrn1 (2.5, 5 and 7.5 pmol) and a fixed concentration (5 pmol) of uniformly labeled *in vitro* transcribed FAD-capped or NAD-capped or triphosphate RNA (pppA-). (D) EMSA using equimolar concentration (5 pmol) of Xrn1 and uniformly labeled *in vitro* transcribed FAD-capped or NAD-capped or pppA-RNAs in the absence and presence of 7 pmol and 14 pmol total yeast RNA as a nonspecific competitor.

### Loss of Xrn1 increases FAD-capped RNA in cells

To evaluate whether Xrn1 hydrolysed the FAD cap within the diphosphate moiety analogous to the class 2 Nudt12 protein (9), or removed the intact FAD, like the class 1 DXO/Rai1 family of proteins (7), FAD cap detection and quantitation (FAD-capQ) was used. FAD-capQ approach detects intact FAD caps released from the 5'-end of RNAs *en masse* (13). Hydrolysis of an increasing concentration of *in vitro* transcribed FAD-capped RNA with Xrn1 released a corresponding increase of FAD which was not observed in the reactions with catalytically dead Xrn1 mutant nor with NAD-capped RNA as expected (Figure 3A). Furthermore, comparison of FAD liberated from FAD-capped

RNA to that of free FAD standard curve demonstrates the major product released was FAD (Supplementary Figure S4). Next, we measured the contribution of Xrn1 deFADding on endogenous FAD-capped RNA. Consistent with a deFADding function for Xrn1 in cells, a statistically significant 2-fold higher level of total FAD cap was detected in the *xrn1Δ* strain relative to the WT strain (Figure 3B). These findings demonstrate Xrn1 is a class I deFADding enzyme that releases the intact FAD moiety, and this activity is also evident in cells.

The evolutionary conservation of Xrn1 deFADding beyond yeast was next assessed by testing recombinant and endogenous human Xrn1. As shown in Figure 3C, recombinant human Xrn1 hydrolyzed FAD-capped RNA, whereas

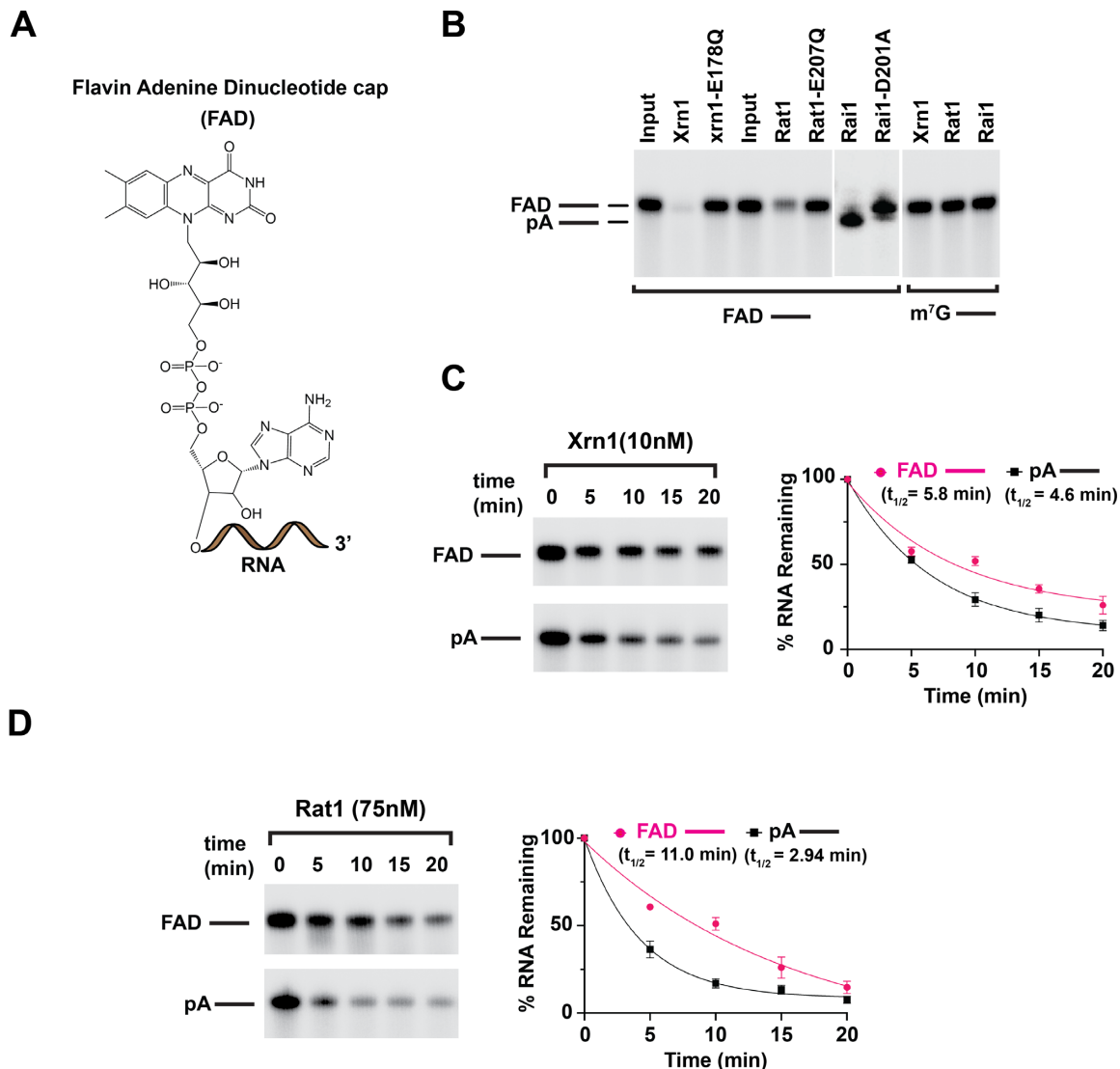


**Figure 2.** Xrn1 and Rat1 are deFADding enzymes. (A) Chemical structure of FAD-capped RNA. (B) Reaction products of *in vitro* deFADding assays with 50 nM recombinant Xrn1, WT, and catalytically inactive (*E178Q*) from *K. lactis* or 100 nM recombinant Rat1, WT or catalytically inactive (*E207Q*) from *S. pombe* or 25 nM Rai1, WT catalytically inactive (*D201A*) (*S. pombe*). Approximately 230 nM uniformly  $^{32}\text{P}$ -labeled monophosphate (pA $^-$ ) or FAD-capped RNA (FAD $^-$ ) where the line denotes the RNA, were used as indicated. Reaction products were resolved on 15% 7M urea PAGE gels. Time-course decay analysis of  $\sim$ 230 nM uniformly  $^{32}\text{P}$ -labeled monophosphate or FAD-capped RNA with the indicated amount of Xrn1 (C) or Rat1 (D) protein are shown. Quantitation of RNA remaining is plotted from three independent experiments with  $\pm$ SD denoted by error bars along with the one phase decay curve.

the catalytically dead E178Q mutant did not. Similarly, the contribution of endogenous human Xrn1 to deFADding in cells was assessed using FAD-capQ. Levels of FAD caps were found to be  $\sim$ 2-fold higher in human HEK293T cells with a CRISPR Cas9-directed disruption of the *Xrn1* gene (30) relative to the WT control cells (Figure 3D) which was comparable to the activity of the DXO deFADding enzyme as previously reported (Figure 3D and (13)). We conclude the deFADding activity of Xrn1 is not restricted to yeast and at least extends to human Xrn1.

#### Highly conserved Histidine 41 in Xrn1 is dispensable for deFADding activity

Disruption of both deFADding and 5'P mediated exonuclease activities by the E178Q mutation in Xrn1 suggests both

activities share catalytic residues for their enzymatic function. To assess whether the two activities could be uncoupled, we generated recombinant Xrn1 proteins with substitution mutations in several key residues within the catalytic center and in the 5'P binding pocket (Supplementary Figure S5A). No significant differences were detected with any of the proteins containing mutations in 4 critical residues in their ability to degrade FAD-capped or 5'P RNA *in vitro* (Supplementary Figure S5B). Unexpectedly, this also included a substitution of Histidine 41 to Alanine (H41A), in contrast to observations with the deNADding activity (11). The H41A mutation could distinguish between deNADding and exonuclease activities where deNADding activity was inhibited with minimal disruption of 5'P hydrolysis (11). Our findings reveal 5'P directed exonuclease activity and deFADding activities share common residues required

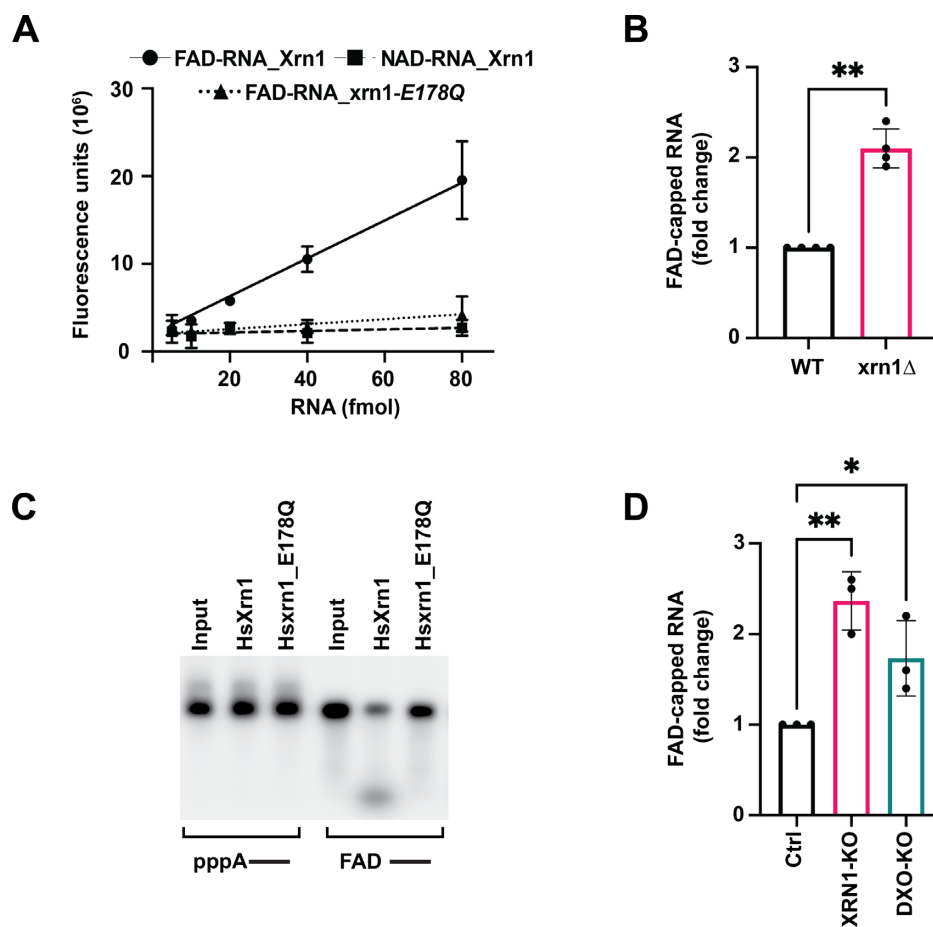


**Figure 3.** Xrn1 deFADs FAD-capped RNAs in both yeast and human cells. (A) FAD-capQ assay using different amounts of *in vitro* transcribed FAD-capped RNA to demonstrate the release of intact FAD upon Xrn1 mediated deFADding. Catalytic-dead mutant of Xrn1, E178Q was used as a control for the Xrn1 reaction and NAD-capped RNA was used as a control for specific detection of FAD in the assay. (B) Total RNAs from WT and *xrn1Δ* were subjected to the FAD-capQ assay to detect total levels of cellular FAD-capped RNA. Data represents average from four independent experiments. Error bars represent  $\pm$  SD with unpaired *t*-test; \*  $P < 0.05$ , \*\*  $P < 0.001$ , \*\*\*  $P < 0.0001$ . (C) Reaction products of *in vitro* deFADding assays with 100nM recombinant human Xrn1 (Hs\_Xrn1) and catalytically inactive (E178Q). (D) Small RNAs (<200 nts) from three biological replicates of HEK293T Ctrl, XRN1-KO and DXO-KO cells were subjected to the FAD-capQ assay to detect total level of cellular FAD-capped RNAs. Data represents average from three independent experiments. Error bars represent  $\pm$  SD with unpaired *t*-test; \*  $P < 0.05$ , \*\*  $P < 0.001$ , \*\*\*  $P < 0.0001$ .

for their catalytic function compared to the action of Xrn1 in deNADding.

### Bacterial 5'-3' exoribonuclease RNase AM is a novel deFADding enzyme

The unexpected finding that both major eukaryotic 5'-3' exoribonucleases Xrn1 and Rat1 possess deFADding and deNADding activity raised the possibility that metabolite cap decapping may be an intrinsic property of 5' end exoribonuclease in another domain. To test this, we assessed the deFADding and deNADding activities of a recently characterized 5'-3' exoribonuclease in *E. coli*, RNase AM (*yciV*) (14,15), which can hydrolyze short RNAs of up to five nucleotides with a 5'P. We were able to expand on the original observations and demonstrate that a 40 nucleotide RNA molecule can also be degraded by RNase AM and further demonstrate the exonuclease activity is processive (Figure 4A). Intriguingly, RNase AM also demonstrated robust deFADding activity, but unlike the two eukaryotic nucleases, RNase AM did not hydrolyze NAD-capped RNA (Figure

4A). Strikingly, RNase AM degraded both FAD-capped and 5'P RNAs at comparable rates *in vitro* (Figure 4B). Additionally, like Xrn1, RNase AM degraded the FAD-capped RNA by removing and releasing the intact FAD as assessed by FAD-capQ (Figure 4C).

The effect of RNase AM on endogenous FAD-capped RNA was next determined. Total RNA from WT or *rnase AM* knockout *E. coli* strains were subjected to FAD-capQ and levels of released FAD detected. As shown in Figure 4D, a statistically significant 1.5-fold higher level of total FAD cap was detected in the *rnase AM* knock out strain relative to the WT strain. Our findings demonstrate that *E. coli* RNase AM can function as a deFADding enzyme in cells.

### Structural analysis of RNase AM

To gain insight into how an exoribonuclease could function as a deFADding enzyme, we attempted to determine the crystal structure of *E. coli* RNase AM in complex with FAD in an effort to elucidate the mechanism for RNase

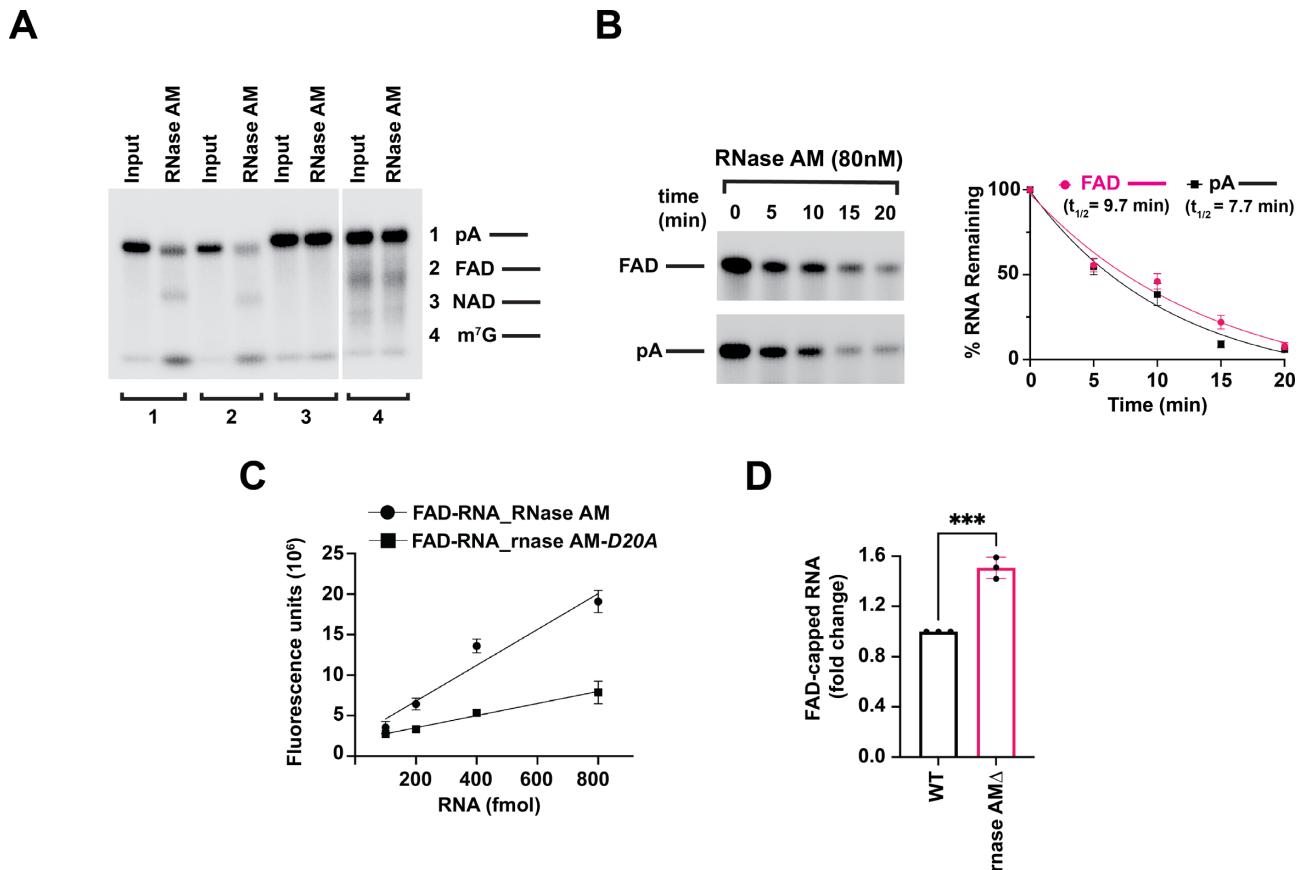


**Figure 4.** RNase AM is a novel deFADding enzyme in *E. coli*. (A) Reaction products of *in vitro* deFADding assays with 100 nM recombinant RNase AM. Uniformly  $^{32}\text{P}$ -labeled monophosphate (pA $^-$ ) or FAD-capped RNA (FAD $^-$ ), NAD-capped (NAD $^-$ ) and  $m^7\text{G}$ -capped ( $m^7\text{G}$  $^-$ ). Reaction products were resolved on 15% 7 M urea PAGE gels. (B) Time-course decay analysis of  $\sim 300$  nM uniformly  $^{32}\text{P}$ -labeled monophosphate or FAD-capped RNA with the indicated amount of RNase AM protein are shown. Quantitation of RNA remaining is plotted from three independent experiments with  $\pm$  SD denoted by error bars along with the one phase decay curve. (C) To demonstrate that RNase AM releases intact FAD upon deFADding like Xrn1 (in Figure 3), FAD-capQ assay using different amount of *in vitro* transcribed FAD-capped RNA was used. Catalytic-dead mutant of RNase AM, D20A was used as control for the reaction. (D) Total RNA from WT and *rnase AM* $\Delta$  were subjected to the FAD-capQ assay to detect total levels of cellular FAD-capped RNA. Data represents an average from three independent biological experiments. Error bars represent  $\pm$  SD with unpaired *t*-test; \*  $P < 0.05$ , \*\*  $P < 0.001$ , \*\*\*  $P < 0.0001$ .

AM monophosphate hydrolysis and deFADding activities. RNase AM expressed in the presence of the iron chelator 2,2'-bipyridyl and  $\text{MnSO}_4$ , to prevent Fe from being the cation in the active site (31), was competent for binding FAD (as determined by thermal shift assay; data not shown). However, no crystals were obtained for RNase AM alone or in the presence of FAD. Good quality crystals were obtained of RNase AM incubated with a dsRNA, and a molecular replacement solution was obtained using the polymerase and histidinol phosphatase (PHP) domain from the *Chromobacterium violaceum* amidohydrolase, CV1693 (PDB: 2YB1) as the search model (24). No density for the RNase AM insertion domain was observed, indicating that the domain is disordered in this crystal. The final structure consists of residues 9–106 and 177–284 and is modeled with three manganese ions ( $\text{Mn}\alpha$ ,  $\text{Mn}\beta$ , and  $\text{Mn}\gamma$ ) and a sulfate molecule in the active site. The refined atomic model contained no RNA and has excellent agreement with the X-ray diffraction data and the expected bond lengths, bond angles and other geometric parameters (Table 1).

RNase AM belongs to the PHP domain family of proteins which is composed of amidohydrolases/phosphoesterases and is present in some DNA polymerases. RNase AM has a distorted ( $\beta/\alpha$ ) $_7$ -barrel fold and a three metal enzyme active site composed of histidines and aspartates/glutamate residues (Figure 5A and D).  $\text{Mn}\alpha$  and  $\text{Mn}\beta$ , which are proposed to coordinate the water for nucleophilic attack are coordinated by residues His13, Glu72 and Asp255, and Glu72, His83 and His198 respectively (Figure 5D).  $\text{Mn}\gamma$  is coordinated by residues Asp20, His45 and His257. The sulfate molecule coordinates all three metals and forms a salt bridge with Arg201, which may stabilize the hydrolysis reaction intermediate. Comparison to the CV1693 product complex containing AMP and  $\text{P}_i$  (24) shows that RNase AM has the same overall fold and active site architecture, and the RNase AM sulfate is in the same position as the phosphate product (Figure 5C and D). Disruption of the active site by the D20A, E72A and D255/H257A mutations resulted in disruption of 5'P and deFADding activities demonstrating the importance of the metals for

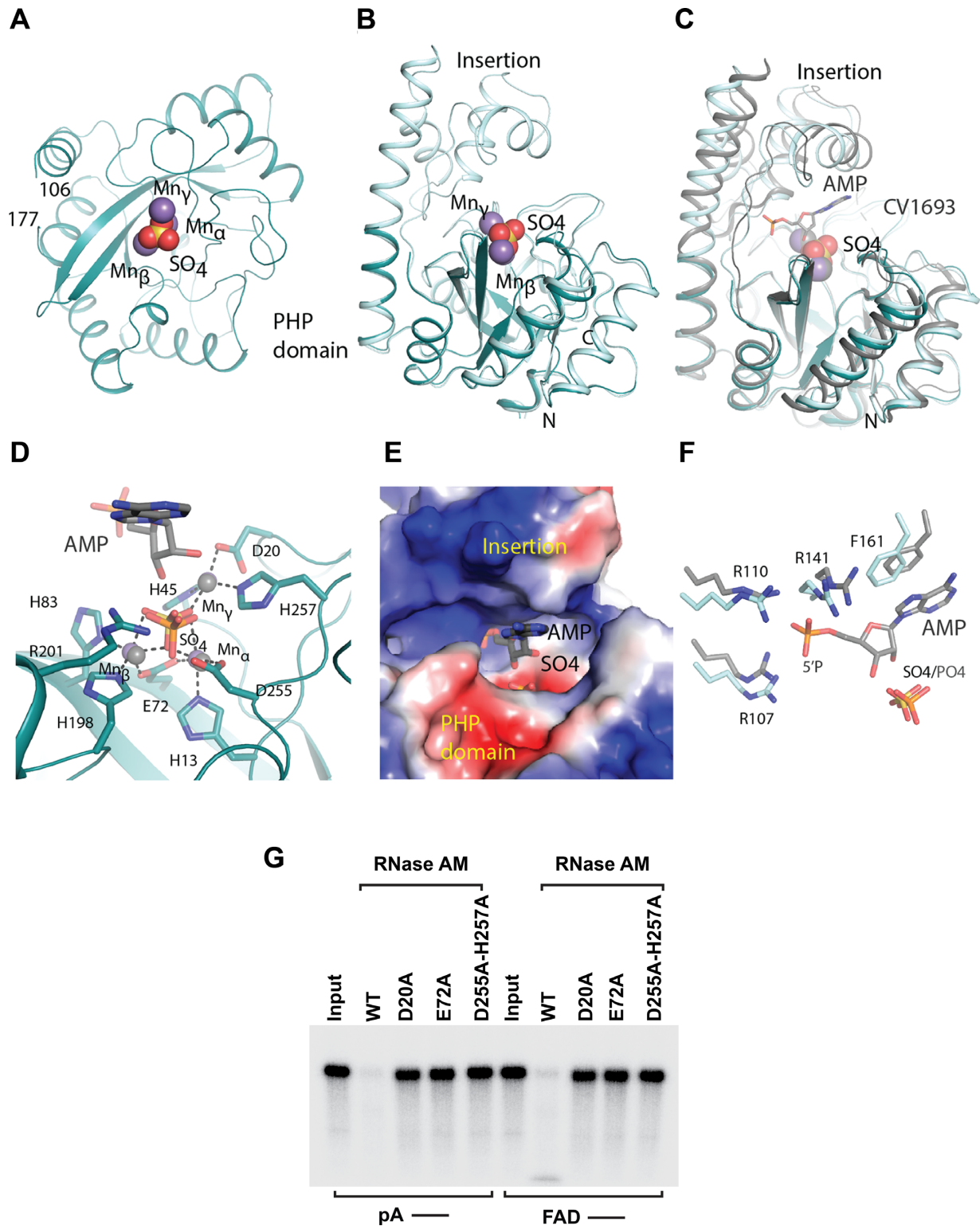


**Figure 5.** Structural and mutagenesis analysis of RNase AM activities. (A) Overall crystal structure of RNase AM PHP domain (teal) with manganese ions (purple) and sulfate (yellow and red) shown as spheres. (B) Overlay of RNase AM crystal structure (teal) with RNase AM from AlphaFold (light blue) showing the insertion domain. (C) Overlay of RNase AM with CV1693 (gray) with AMP from CV1693 shown as sticks. (D) The active site of RNase AM showing the coordination of the three manganese ions and sulfate to the active site residues (sticks). AMP and manganese (gray) and the phosphate (orange and red) from the overlay with CV1693 are shown. (E) Electrostatic potential mapped onto the surface of RNase AM showing the positively charged region where the 5'P from CV1693 AMP (gray) is buried. (F) Comparison of binding of AMP (gray) between RNase AM and CV1693 showing positive conservation of the residues that interact with AMP. (G) Reaction products of *in vitro* deFADding assays with 100 nM recombinant RNase AM and putative catalytically inactive point mutants. Uniformly <sup>32</sup>P-labeled monophosphate (pA-) or FAD-capped RNA (FAD-) are indicated. Reaction products were resolved on 15% 7 M urea PAGE gels

these activities (Figure 5G). Together these data indicate that RNase AM uses the same mechanism as CV1693 for hydrolysis.

To gain further insight into the 5'P and deFADding activities of RNase AM we used the full-length RNase AM model from AlphaFold (RNase AM<sub>AF</sub>) (32). RNase AM<sub>AF</sub> and the RNase AM PHP crystal structure align well with an RMSD of 0.58 Å and aligns with CV1693 with an RMSD of 1.71 Å (Figure 5B and C). Comparison of RNase AM<sub>AF</sub> with CV1693 shows that the 5' phosphate of the CV1693 AMP (which represents the first nucleotide of 5'P RNA or the adenosine moiety from FAD) is buried in a positively charged cavity between the PHP and insertion domains comprised primarily of residues Arg107, Arg110, and Arg141 (Figures 5E and F). Similar to CV1693, a stacking interaction can be made between the 5' adenine base and Phe161. This mode of binding may explain 5'P activity of RNase AM; however, the buried position of the 5'P indicates FAD cannot bind in the same manner, suggesting RNase AM utilizes distinct binding modes for 5'P and FAD RNA recognition.

## DISCUSSION

The 5' cap of RNA is a critical determinant of the RNA fate. The N7-methyl-Guanosine (m<sup>7</sup>G) on the 5' end of mRNAs in eukaryotes is the most common and well-studied 5' RNA cap (33). Recent highly sensitive chemical analysis of the 5' ends of the RNA from prokaryotes, eukaryotes and pathogenic viruses has uncovered the presence of nucleotide metabolite caps (12). These can consist of adenosine derived metabolites—NAD, FAD, dpCoA and uracil derived sugars—UDP-GlcNAc and UDP-Glc. Although NAD caps have been shown to promote RNA turnover, whether additional metabolite caps contribute to RNA stability or other RNA processing events remains to be determined. To begin exploring a potential function of FAD caps, we characterized proteins from the model organism, *S. cerevisiae* that can interact with the FAD cap. Surprisingly, the predominant FAD-cap interacting proteins were the 5'P dependent exoribonucleases that also possessed deFADding activity. Moreover, we demonstrated that the deFADding activity of 5' end exoribonucleases was apparent in bacteria, yeast and humans is indicative of convergent evolution of this intrinsic property. RNase AM is so far the only 5'-3' exoribonuclease known in *E. coli*, the enzymatic activity of which has been shown to be essential for the processing of bacterial ribosomal RNA (15).

We recently reported that both Xrn1 and Rat1 possess deNADding activity (11) in addition to their canonical monophosphate RNA hydrolysis activity (29,34). We further uncovered that that the deNADding activity of Xrn1 is essential for mitochondrial NAD-capped RNA homeostasis (11). Remarkably, the deFADding activity of both Xrn1 and Rat1 was found to be more robust than their deNADding activity and as potent as their canonical monophosphate RNA hydrolysis activity. In contrast, the RNase AM exoribonuclease was more selective and exhibited deFADding, but not deNADding activity. Although we were able to uncouple the deNADding activity of Xrn1 from its monophosphate RNA decay by utilising a specific point mutation in the catalytic pocket, H41A, all our at-

tempts to separate deFADding from monophosphate RNA hydrolysis for both Xrn1 and RNase AM were not fruitful. We screened several point mutations of residues that form the catalytic domain of both Xrn1 and RNase AM, along with the residues proximal to catalytic domain, but unfortunately could not untangle the enzymatic activities. Nevertheless, this implied that both activities are apparently mediated by identical residues and are inherent to 5'-3' exoribonucleases. Co-crystal structures of Xrn1-FAD and RNase AM-FAD will be necessary to discern the precise binding mode of this dinucleotide and the molecular basis of its deFADding activity by exoribonucleases. Moreover, RNase AM is conserved in many pathogenic bacteria including *Klebsiella pneumoniae*, *Salmonella enterica*, *Vibrio cholerae*, *Yersinia pestis* (14) and the active site molecular details revealed in the present study could prove significant in small molecule targeting approaches.

Our analysis of the levels of FAD capped RNA isolated from both yeast and human Xrn1 knock out cells and RNase AM knock out *E. coli* cells assessed by FAD-capQ analysis validated that these 5'-3' exoribonucleases can impact levels of total FAD-capped RNA in cells. These findings establish Xrn1 and RNase AM as novel deFADding enzymes adding to the existing list of enzymes that function in FAD cap decapping in cells including Rai1 (13), its mammalian homolog DXO, and Nudt16 (10). We also note that relative to NAD caps (12), FAD cap levels are significantly lower in yeast, human and bacterial cells as determined with FAD-capQ, which correlates well with the relative amount of free NAD and FAD in the cells (35,36).

At present it is difficult to discern any potential biological function of FAD caps. Unlike a role for NAD caps in mitochondrial NAD homeostasis which was deciphered by uncoupling 5'P directed and NAD-cap directed decay (11), we were unable to separate the 5'P and deFADding activities (Supplementary Figure S5). Furthermore, although our initial objective was to find high affinity FAD cap-binding proteins that could be used to selectively identify FAD-capped RNAs, we surprisingly only identified nucleases rather than *bona fide* high affinity cap binding proteins. The association of FAD caps with nucleases may suggest the cap functions as a mark for targeted decay analogous to the NAD cap in mammals. Further analysis to delineate a possible function for FAD caps will require novel methodologies that can selectively isolate and identify cellular RNAs that harbor this noncanonical cap.

## DATA AVAILABILITY

Atomic coordinates and structure factors for the reported crystal structures have been deposited with the Protein Data Bank under accession number 7UG9. Mass spectrometry data has been deposited at MassIVE repository with the Mass Spectrometry Accession Number: MSV000089147.

## SUPPLEMENTARY DATA

Supplementary Data are available at NAR Online.

## ACKNOWLEDGEMENTS

We would like to thank Dr Britt Glausinger (University California Berkley) for providing the HEK293T XRN1 knock-

out cell line. We are grateful to Dr Joanna Kowalska (University of Warsaw) for providing the FAD3'P dinucleotide. We also thank Dr Haiyan Zheng (Rutgers University) for her extensive assistance in the analysis of mass spectrometry data.

## FUNDING

National Institutes of Health NIGMS [R35GM118093 to L.T., GM126488 to M.K.]; Northeastern Collaborative Access Team beamlines, which are funded by the National Institute of General Medical Sciences from the National Institutes of Health [P30 GM124165]; Advanced Photon Source; U.S. Department of Energy (DOE) Office of Science User Facility operated for the DOE Office of Science by Argonne National Laboratory [DE-AC02-06CH11357]. Funding for open access charge: NIGMS [GM126488].

*Conflict of interest statement.* None declared.

## REFERENCES

- Berger, S.L. and Sassone-Corsi, P. (2016) Metabolic signaling to chromatin. *Cold Spring Harbor Perspect. Biol.*, **8**, a019463.
- Li, X., Egervari, G., Wang, Y., Berger, S.L. and Lu, Z. (2018) Regulation of chromatin and gene expression by metabolic enzymes and metabolites. *Nat. Rev. Mol. Cell Biol.*, **19**, 563–578.
- Cahova, H., Winz, M.L., Hofer, K., Nubel, G. and Jaschke, A. (2015) NAD captureSeq indicates NAD as a bacterial cap for a subset of regulatory RNAs. *Nature*, **519**, 374–377.
- Walters, R.W., Matheny, T., Mizoue, L.S., Rao, B.S., Muhlrud, D. and Parker, R. (2017) Identification of NAD<sup>+</sup> capped mRNAs in *Saccharomyces cerevisiae*. *Proc. Natl. Acad. Sci. U.S.A.*, **114**, 480–485.
- Wang, Y., Li, S., Zhao, Y., You, C., Le, B., Gong, Z., Mo, B., Xia, Y. and Chen, X. (2019) NAD(+) capped RNAs are widespread in the arabidopsis transcriptome and can probably be translated. *Proc. Natl. Acad. Sci. U.S.A.*, **116**, 12094–12102.
- Zhang, H., Zhong, H., Zhang, S., Shao, X., Ni, M., Cai, Z., Chen, X. and Xia, Y. (2019) NAD tagSeq reveals that NAD(+) capped RNAs are mostly produced from a large number of protein-coding genes in arabidopsis. *Proc. Natl. Acad. Sci. U.S.A.*, **116**, 12072–12077.
- Jiao, X., Doamekpor, S.K., Bird, J.G., Nickels, B.E., Tong, L., Hart, R.P. and Kiledjian, M. (2017) 5' end nicotinamide adenine dinucleotide cap in human cells promotes RNA decay through DXO-Mediated deNADding. *Cell*, **168**, 1015–1027.
- Bird, J.G., Zhang, Y., Tian, Y., Panova, N., Barvik, I., Greene, L., Liu, M., Buckley, B., Krasny, L., Lee, J.K. *et al.* (2016) The mechanism of RNA 5' capping with NAD<sup>+</sup>, NADH and desphospho-CoA. *Nature*, **535**, 444–447.
- Grudzien-Nogalska, E., Wu, Y., Jiao, X., Cui, H., Mateyak, M.K., Hart, R.P., Tong, L. and Kiledjian, M. (2019) Structural and mechanistic basis of mammalian nudt12 RNA deNADding. *Nat. Chem. Biol.*, **15**, 575–582.
- Sharma, S., Grudzien-Nogalska, E., Hamilton, K., Jiao, X., Yang, J., Tong, L. and Kiledjian, M. (2020) Mammalian nudix proteins cleave nucleotide metabolite caps on RNAs. *Nucleic Acids Res.*, **48**, 6788–6798.
- Sharma, S., Yang, J., Grudzien-Nogalska, E., Shivas, J., Kwan, K.Y. and Kiledjian, M. (2022) Xrn1 is a deNADding enzyme modulating mitochondrial NAD-capped RNA. *Nat. Commun.*, **13**, 889.
- Wang, J., Chew, B.L.A., Lai, Y., Dong, H.P., Xu, L., Balamkundu, S., Cai, W.M., Cui, L., Liu, C.F., Fu, X.Y. *et al.* (2019) Quantifying the RNA cap epitranscriptome reveals novel caps in cellular and viral RNA. *Nucleic Acids Res.*, **47**, e130.
- Doamekpor, S.K., Grudzien-Nogalska, E., Mlynarska-Cieslak, A., Kowalska, J., Kiledjian, M. and Tong, L. (2020) DXO/Rail enzymes remove 5'-end FAD and dephospho-CoA caps on RNAs. *Nucleic Acids Res.*, **48**, 6136–6148.
- Ghodge, S.V. and Raushel, F.M. (2015) Discovery of a previously unrecognized ribonuclease from *Escherichia coli* that hydrolyzes 5'-Phosphorylated fragments of RNA. *Biochemistry*, **54**, 2911–2918.
- Jain, C. (2020) RNase AM, a 5' to 3' exonuclease, matures the 5' end of all three ribosomal RNAs in *E. coli*. *Nucleic Acids Res.*, **48**, 5616–5623.
- Morrissey, J.H. (1981) Silver stain for proteins in polyacrylamide gels: a modified procedure with enhanced uniform sensitivity. *Anal. Biochem.*, **117**, 307–310.
- Craig, R. and Beavis, R.C. (2004) TANDEM: matching proteins with tandem mass spectra. *Bioinformatics*, **20**, 1466–1467.
- Gupta, N., Bandeira, N., Keich, U. and Pevzner, P.A. (2011) Target-decoy approach and false discovery rate: when things may go wrong. *J. Am. Soc. Mass. Spectrom.*, **22**, 1111–1120.
- Song, M.G., Bail, S. and Kiledjian, M. (2013) Multiple nudix family proteins possess mRNA decapping activity. *RNA*, **19**, 390–399.
- Edelheit, O., Hanukoglu, A. and Hanukoglu, I. (2009) Simple and efficient site-directed mutagenesis using two single-primer reactions in parallel to generate mutants for protein structure-function studies. *BMC Biotechnol.*, **9**, 61.
- Collart, M.A. and Oliviero, S. (2001) Preparation of yeast RNA. *Curr. Protoc. Mol. Biol.*, **Chapter 13**, Unit 13.12.
- Leppke, K., Schott, J., Reitter, S., Poetz, F., Hammond, M.C. and Stoecklin, G. (2013) Roquin promotes constitutive mRNA decay via a conserved class of stem-loop recognition motifs. *Cell*, **153**, 869–881.
- Kabsch, W. (2010) Integration, scaling, space-group assignment and post-refinement. *Acta Cryst.*, **D66**, 133–144.
- Cummings, J.A., Vetting, M., Ghodge, S.V., Xu, C., Hillerich, B., Seidel, R.D., Almo, S.C. and Raushel, F.M. (2014) Prospecting for unannotated enzymes: discovery of a 3',5'-nucleotide bisphosphate phosphatase within the amidohydrolase superfamily. *Biochemistry*, **53**, 591–600.
- McCoy, A.J., Grosse-Kunstleve, R.W., Adams, P.D., Winn, M.D., Storoni, L.C. and Read, R.J. (2007) Phaser crystallographic software. *J. Appl. Crystallogr.*, **40**, 658–674.
- Adams, P.D., Grosse-Kunstleve, R.W., Hung, L.W., Ioerger, T.R., McCoy, A.J., Moriarty, N.W., Read, R.J., Sacchettini, J.C., Sauter, N.K. and Terwilliger, T.C. (2002) PHENIX: building new software for automated crystallographic structure determination. *Acta Crystallogr. D Biol. Crystallogr.*, **58**, 1948–1954.
- Emsley, P. and Cowtan, K. (2004) Coot: model-building tools for molecular graphics. *Acta Crystallogr. D Biol. Crystallogr.*, **60**, 2126–2132.
- Xiang, S., Cooper-Morgan, A., Jiao, X., Kiledjian, M., Manley, J.L. and Tong, L. (2009) Structure and function of the 5'→3' exoribonuclease rat1 and its activating partner rail. *Nature*, **458**, 784–788.
- Larimer, F.W., Hsu, C.L., Maupin, M.K. and Stevens, A. (1992) Characterization of the XRN1 gene encoding a 5'→3' exoribonuclease: sequence data and analysis of disparate protein and mRNA levels of gene-disrupted yeast cells. *Gene*, **120**, 51–57.
- Gilbertson, S., Federspiel, J.D., Hartenian, E., Cristea, I.M. and Glaunsinger, B. (2018) Changes in mRNA abundance drive shuttling of RNA binding proteins, linking cytoplasmic RNA degradation to transcription. *Elife*, **7**, e37663.
- Ghodge, S.V. and Raushel, F.M. (2015) Discovery of a previously unrecognized ribonuclease from *Escherichia coli* that hydrolyzes 5'-Phosphorylated fragments of RNA. *Biochemistry*, **54**, 2911–2918.
- Jumper, J., Evans, R., Pritzel, A., Green, T., Figurnov, M., Ronneberger, O., Tunyasuvunakool, K., Bates, R., Zidek, A., Potapenko, A. *et al.* (2021) Highly accurate protein structure prediction with AlphaFold. *Nature*, **596**, 583–589.
- Furuichi, Y. (2015) Discovery of m(7)G-cap in eukaryotic mRNAs. *Proc. Jpn. Acad. Ser. B. Phys. Biol. Sci.*, **91**, 394–409.
- Amberg, D.C., Goldstein, A.L. and Cole, C.N. (1992) Isolation and characterization of RAT1: an essential gene of *Saccharomyces cerevisiae* required for the efficient nucleocytoplasmic trafficking of mRNA. *Genes Dev.*, **6**, 1173–1189.
- Canto, C., Menzies, K.J. and Auwerx, J. (2015) NAD(+) metabolism and the control of energy homeostasis: a balancing act between mitochondria and the nucleus. *Cell Metabolism*, **22**, 31–53.
- Huhner, J., Ingles-Prieto, A., Neuss, C., Lammerhofer, M. and Janovjak, H. (2015) Quantification of riboflavin, flavin mononucleotide, and flavin adenine dinucleotide in mammalian model cells by CE with LED-induced fluorescence detection. *Electrophoresis*, **36**, 518–525.